LABORATORY TESTING OF THE FACTOR ANALYSIS-TARGET TRANSFORMATION METHOD FOR MINERAL DETECTION AT LOW ABUNDANCE FROM VISIBLE-INFRARED HYPERSPECTRAL DATA J. F. Mustard[1], J. D. Tarnas[1] and M. Parente[2], [1]Department of Earth, Environmental and Planetary Sciences, Brown University, Providence RI 02912. (john_mustard@brown.edu) [2]Dept. of Electrical and Computer Engineering, University of Massachusetts Amherst, MA 01003.

Introduction: What is present and how much? Mineral detection and abundance determination are important goals of quantitative analysis of hyperspectral visible to short-wave infrared (i.e. 0.4-2.6 μm) remotely sensed data. From innovations in data analysis over the past decade new approaches to mineral detection and abundance have emerged [1, 2] that are very promising but have not been rigorously tested in laboratory settings. Specifically laboratory test are required to definitively exclude false positive detections and assess abundance determination capabilities in low abundance settings. We will present the first results of laboratory experiments specifically designed to address mineral detection techniques.

Methods: Mineral presence has commonly been determined by keying on diagnostic absorption features, keying on the position, strength and shape (e.g. width) of absorptions in remote and laboratory spectra using spectral parameters [3] to guide the selection of remotely acquired spectra to compare to laboratory spectra [e.g. 4, 5]. However this approach requires a pre-determination of likely minerals to be present, is not flexible or extendable to diverse situations and can be severely hampered by instrument noise and calibration artifacts.

The Factor Analysis Target Transformation (FATT) approach to identify mineral presence is a promising technique to identify minerals in hyperspectral data where the abundances may be low and in the presence of instrumental noise and artifacts of calibration [2]. The FATT approach extracts the first 10 eigenvectors from a hyperspectral data set. These eignvectors are then linearly fit to laboratory spectra of candidate minerals. A goodness of fit test (e.g. root mean square error) can then be used to assess if that mineral is present [2]. While this approach has shown good utility, there are questions as to the number of eigenvectors require and appropriate metrics for goodness of fit. It is also not known the factors that could lead to false positive detections of missed identifications. Furthermore, it is not required that the presence of the mineral phase in question be observed using typical approaches (e.g. [4]). Finally, FATT does not provide estimates of fractional abundances.

We have designed a robust laboratory experiment to test the FATT approach using a laboratory imaging spectrometer. Samples will be placed in a special tray, painted black (0.03% reflectance 0.3-2.8 μm), that is 30x30x1 cm in size and divided into 9 sectors (Figure 1). The tray's 1 cm depth will be filled with a novel new Mars simulant created by K. Cannon [6]. This simulant, a chemical and mineralogic analog to the global basaltic soil, is based on the Rocknest measurements. It is an excellent spectroscopic analog to the global basaltic soil and is a perfect material for our experiments.

The Mars soil simulant is mixed with 8 different hydrated endmembers (Figure 1) that have been proposed to be on Mars based on observations with CRISM and OMEGA data [7] and detected using parameter maps and comparisons of remotely detected spectra with library spectra. The endmembers and simulant are mixed by mass fraction in proportions designed to test the detection thresholds of the algorithms. Specifically at 1%, 2.5%, 5% and 10%. The volume fraction are determined as well. The presence of the target minerals should be readily evident at the 10% mixture abundance using standard mineral detection techniques but where the lower detection limit exists is currently not known.

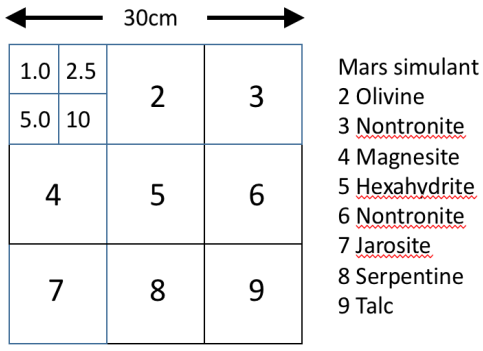

Figure 1: Schematic of the targets of mixing experiment with imaging spectroscopy

The upper left sector is filled with only Mars simulant as the experiment "blank". Each of the other 8 sectors are divided into four segments. The four segments are filled with mixtures of Mars simulant and 1.0, 2.5, 5.0 and 10.0% by mass of the target minerals (Figure 1). The fully loaded sample tray thus has 32 mixtures that should stress the algorithms.

Data Acquisition: The sample tray is measured with the Brown University Headwall Imaging Spectrometer. The Headwall imaging spectrometer consists of a visible-near infrared and short-wave infrared components, bore-sighted through the same fore optics. Together they provide optical observations across the

wavelength range 400 – 2500 nm. The VNIR instrument collects measurements in the 400 – 1000 nm region using a Si detector with 1600 spatial pixels and 372 spectral pixels. The spectral sampling interval is 1.61 nm and the full width at half maximum (FWHM) is 1.6 nm. The VNIR has an angular instantaneous field of view (IFOV) of 0.096 degrees or 1.687 mrad with a full field of view (FFOV) of 24.3 degrees. The SWIR instrument measures the 1000 – 2500 nm region using a HgCdTe detector with 384 spatial pixels and 167 spectral pixels. The spectral sampling interval is 8.98 nm and the FWHM is 9 nm. The lens on the SWIR instrument produces an angular FFOV and IFOV of 24° and 6.748 mrad respectively. Both instruments are mounted inside an aluminum frame with a data system running software that controls the operation of both sensors and stores data on a 1 Tb solid state drive (SSD). Light entering the VNIR and SWIR lenses first passes through a dichroic filter that transmits wavelengths ≥ 1000 nm to the SWIR instrument and reflects wavelengths in the 400 – 1000 nm range to the VNIR instrument. The VNIR and SWIR instruments are boresight aligned.

In the laboratory the spectrometer is fixed 80 cm above a translation table that moves across the field of view at a rate synched with the Headwall frame rate to acquire square pixels. Example data are shown in Figure 2. The field of view of the instrument is illuminated by a quartz halogen lamp and there is a fixed Spectralon® target along one end of the translation table for calibration. The data are calibrated to reflectance by subtracting the instrument dark current from the sample and calibration panel data and dividing the sample data by the calibration panel. In this geometry the pixel size is 0.5 mm in the visible-near infrared (VNIR) (0.38-1.01 µm) and 2.0 mm in the shortwave infrared (SWIR) (0.95-2.55 µm). This translates to effectively 100x100 VNIR and 25x25 SWIR pixels for each all segment on the sample tray, more than enough pixels to build a robust statistical data base to test the methods.

Results:

The initial result of application of the factor analysis methods to the Oman sample in Figure 2 demonstrate that the target minerals calcite and serpentine can be detected with no false positives. But this test is not necessarily realistic and does not stress the detection capabilities sufficiently. To better demonstrate the capabilities data and results will be shown at the conference using the laboratory mixtures in the set up shown in Figure 1.

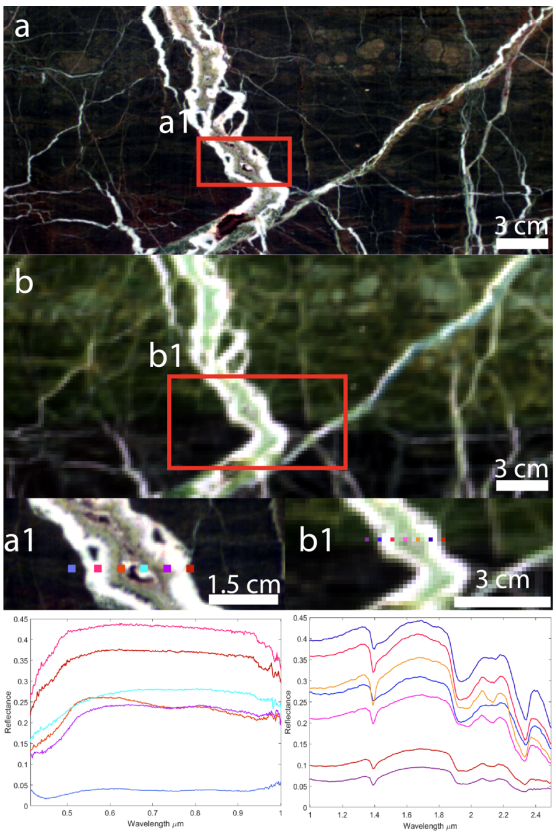

Figure 2. (a) VNIR 0.05 mm/pixel and (b) SWIR 2.0 mm/pixel images of sample from the Oman ophiolite. a1 and b1 are close ups of the red boxes. Minerals present and detected with spectroscopy are serpentine in the dark background/matrix, Ca-carbonate in the white veins and in the grey material within the white veins is serpentine. Color dots correspond to same colored spectra. All calcite spectra show evidence for mixing with serpentine.

References: [1] Lapotre, M., et al. (2017), *J. Geophys. Res. - Planets*, 10.1002/2016JE005133. [2] Thomas, N. H., and J. L. Bandfield. Icarus 291 (2017): 124-135. [3] Viviano-Beck, C. E., F. P. Seelos, S. L. Murchie, E. G. Kahn, K. D. Seelos, H. W. Taylor, K. Taylor et al. *J. of Geophys. Res.-Planets* 119, no. 6 (2014): 1403-1431.[4] Mustard, J. F., et al., *Nature* 454.7202 (2008): 305. [5] Pieters, C. M, et al. *Science* 326.5952 (2009): 568-572. [6] Cannon, K. M., et al. *Icarus* 317 (2019): 470-478. [7] Ellmann, B. L. and C. S. Edwards, *Geology* 43, no. 10 (2015): 863-866. 2015.